



Causes of extreme 2020 Meiyu-Baiu rainfall: a study of combined effect of Indian Ocean and Arctic

Xiaodan Chen¹ · Zhiping Wen^{1,2,3} · Yuanyuan Song⁴ · Yuanyuan Guo¹

Received: 21 November 2021 / Accepted: 28 March 2022 / Published online: 14 June 2022
© The Author(s) 2022

Abstract

A record-breaking Meiyu-Baiu rainfall hit East Asia in June–July 2020. The warm Indian Ocean (IO) has been identified as a primary cause, but it cannot explain the heavy rainfall in July, a striking characteristic of the 2020 Meiyu-Baiu rainfall. A remarkable retreat of Arctic sea ice in the late spring and early summer of 2020 also promoted Meiyu-Baiu rainfall by favoring North Asian blockings and cold air outbreaks. However, its importance compared with IO warming is unclear. Our result shows that the abundant moisture supply to the 2020 Meiyu-Baiu rainfall mainly stems from anomalous meridional wind convergence, while the excessive ascending motions are due to warm advection tied to enhanced mid-troposphere westerlies. AGCM experiments are used to examine the relative importance of IO warming and Arctic sea ice anomalies. In June, IO warming is responsible for the atmospheric circulation anomalies around the Meiyu-Baiu region and accounts for ~75% of the Meiyu-Baiu rainfall anomalies, despite the Arctic sea-ice loss explaining most circulation anomalies over Eurasian high latitudes. In July, both IO warming and Arctic sea-ice loss are necessary for meridional convergence, enhanced westerlies, and thus the heavy rainfall over the Meiyu-Baiu region. Their effects are interdependent rather than additive. Strong IO warming is rarely observed alongside severe Arctic sea-ice loss before 2020 because of their discordant interannual variations. In the future, the combined effects of IO warming and Arctic sea-ice loss on the Meiyu-Baiu rainfall may become more pronounced as their long-term trends continue.

Keywords Meiyu-Baiu rainfall · Indian Ocean · Arctic sea ice · Extreme precipitation

1 Introduction

In early summer, the convergence of the East Asian summer monsoon and the cold air from higher latitudes creates a quasi-stationary front from central-eastern China to Japan. The resulting zonally extended rain belt typically begins in

mid-June and runs into mid-July, having a major impact on East Asia, a densely populated area (Tao and Chen 1987; Ninomiya and Akiyama 1992; Ding et al. 2020). It is known as Meiyu in China, Changma in Korea, and Baiu in Japan.

Due to the extreme Meiyu-Baiu rainfall in June–July 2020, the mid-lower reaches of the Yangtze River in China and the southwest of Japan suffered severe floods, landslides, and urban waterlogging (Takaya et al. 2020; Ueda et al. 2021; Zhou et al. 2021). The accumulated precipitation in the mid-lower reaches of the Yangtze River broke the observational record since 1961 (Chen et al. 2020) and resulted in a massive economic loss of over 170 billion Chinese Yuan (Liang et al. 2021). The intense rainfall in Kyushu island of Japan led to at least 40 deaths, forcing hundreds of thousands of people to evacuate (NASA 2020).

The extreme 2020 Meiyu-Baiu rainfall exhibits a one-week earlier onset, a two-week later retreat, and strong spatial overlap (Chen et al. 2020; Ding et al. 2021). Such an extraordinarily sustained and stationary Meiyu-Baiu front suggests stable atmospheric circulation anomalies in East

✉ Zhiping Wen
zpwen@fudan.edu.cn

¹ Department of Atmospheric and Oceanic Sciences and Institute of Atmospheric Sciences, Fudan University, Shanghai, China

² Innovation Center of Ocean and Atmosphere System, Zhuhai Fudan Innovation Research Institute, Zhuhai 518057, China

³ Jiangsu Collaborative Innovation Center for Climate Change, Zhenjiang, China

⁴ CAS Key Laboratory of Regional Climate-Environment for Temperate East Asia, Institute of Atmospheric Physics, Chinese Academy of Sciences, and University of Chinese Academy of Sciences, Beijing, China

Asia. As shown in Fig. 1a, an anticyclone anomaly is found over the Northwest Pacific in June–July 2020. It boosts southwesterly winds towards the Meiyu-Baiu region in the lower troposphere and intensifies moisture and heat transport (Ding et al. 2021; Li et al. 2021; Zhou et al. 2021). On the other hand, a high-pressure anomaly occupies the East Asian high latitudes (Fig. 1a and Chen et al. 2021; Ding et al. 2021). It is contained in a “two ridges and one trough” pattern across Eurasian high latitudes (Fig. 1a), which is a favorable pattern for the persistent heavy rainfall in central-eastern China (Chen and Zhai 2014). The region of the high-pressure anomaly (highlighted by the grey box in Fig. 1a) experienced excessive atmospheric blockings during June and July 2020 (Chen et al. 2021). A remarkable feature of the 2020 Meiyu-Baiu rainfall is that the accumulated precipitation in July is extraordinarily high (Fig. 1b), which rarely happened in the past (Fig. 1c). Averaged over the Meiyu-Baiu region, the accumulated precipitation anomaly in July is more than twice that in June (Fig. 1c). Forecasting models successfully predicted the rainfall in June but failed in July (Liu et al. 2020; Qiao et al. 2021), indicating an insufficient understanding of the Meiyu-Baiu rainfall in July 2020.

Previous studies found that the excessive Meiyu-Baiu rainfall was mostly a result of El Niño in the preceding winter (e.g., Huang and Wu 1989; Tanaka 1997). However, no El Niño event was observed in winter 2019, notwithstanding the central Pacific exhibits mild warming (Takaya

et al. 2020; Zhou et al. 2021). This moderate-to-normal El Niño-Modoki (Ashok et al. 2007; Marathe et al. 2015) from the summer of 2019 (Ratna et al. 2021) followed by a very strong Indian Ocean Dipole (IOD) mode (Saji et al. 1999) has been suggested to generate downwelling and westward-propagating oceanic Rossby waves, which deepen the thermocline in the southwestern Indian Ocean and sustain warm sea surface temperature (SST) in the Indian Ocean (IO) (e.g. Saji et al. 1999; Saji 2018; Kucharski et al. 2020; Zhou et al. 2021). This is together with an overall warming trend over the IO in recent decades (Saji et al. 2006; Marathe et al. 2021; Guo et al. 2021; Pan et al. 2021), resulting in a strong IO warming in the early summer of 2020 (Fig. 2c, f). Since the long-term SST trend in tropical IO is characterized by a basin-wide uniform warming (Tang et al. 2021), the enhanced warming in the southwestern IO in 2020 (Fig. 2c) is largely from the interannual variations (Fig. 2d). However, we find that the long-term trend and interannual variations contribute equally to the domain-averaged warming over the tropical IO (Fig. 2h) in the spring and summer of 2020, in agreement with previous studies (Tang et al. 2021; Pan et al. 2021). Many observational and modeling studies suggested the IO warming in 2020 early summer is a primary cause of the extreme Meiyu-Baiu rainfall in 2020 (e.g., Fang et al. 2021; Guo et al. 2021; Pan et al. 2021; Tang et al. 2021; Ueda et al. 2021; Zheng and Wang 2021; Zhou et al. 2021). It drives an anomalous anticyclone over the northern IO and

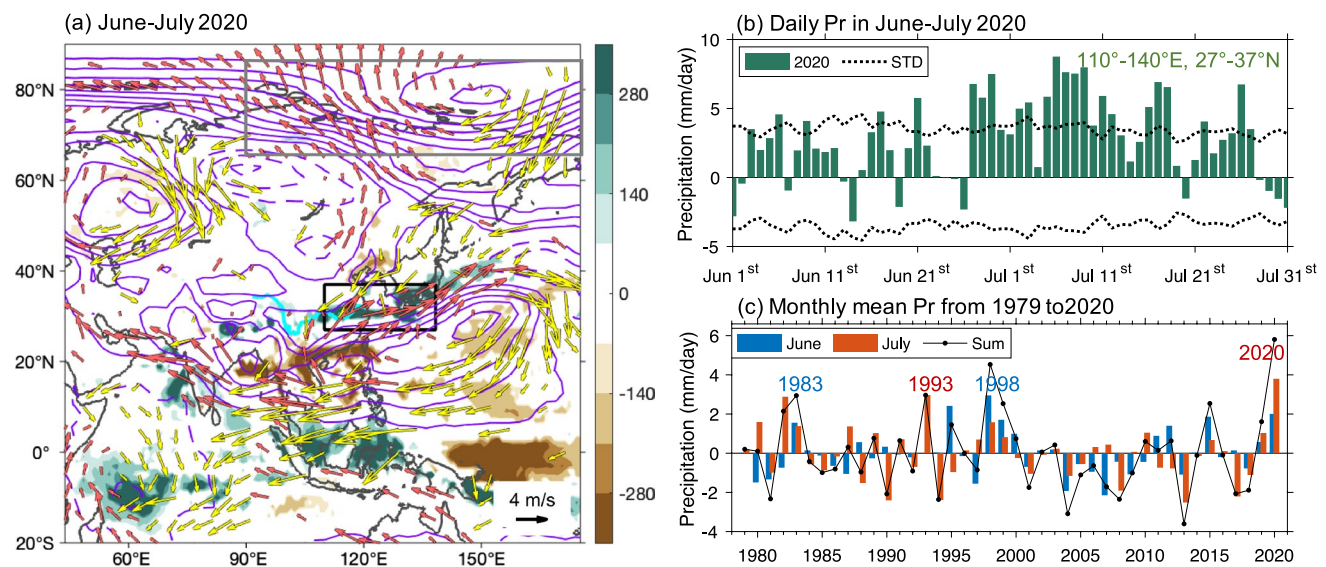


Fig. 1 **a** Anomalies of accumulated precipitation (shading; mm) during June–July 2020 and the associated time-averaged anomalies of 850 hPa geopotential height (contours; interval=50 gpm, with dashed lines for negative values) and horizontal winds (vectors; with red for southerlies and yellow for northerlies). The black box highlights the Meiyu-Baiu region (110°–140° E, 27°–37° N). The grey box highlights the region with a positive geopotential anomaly

in June through July (90°–170° E, 65°–85° N) and the excessive atmospheric blocking frequency (Chen et al. 2021). **b** The daily evolution of precipitation anomaly averaged over the Meiyu-Baiu region from June 1st to July 31st 2020. The black dotted lines denote the range of standard deviation. **c** Monthly precipitation anomaly averaged over the Meiyu-Baiu region in June (blue bar) and July (red bar) from 1979 to 2020, as well as their sum (black dots)

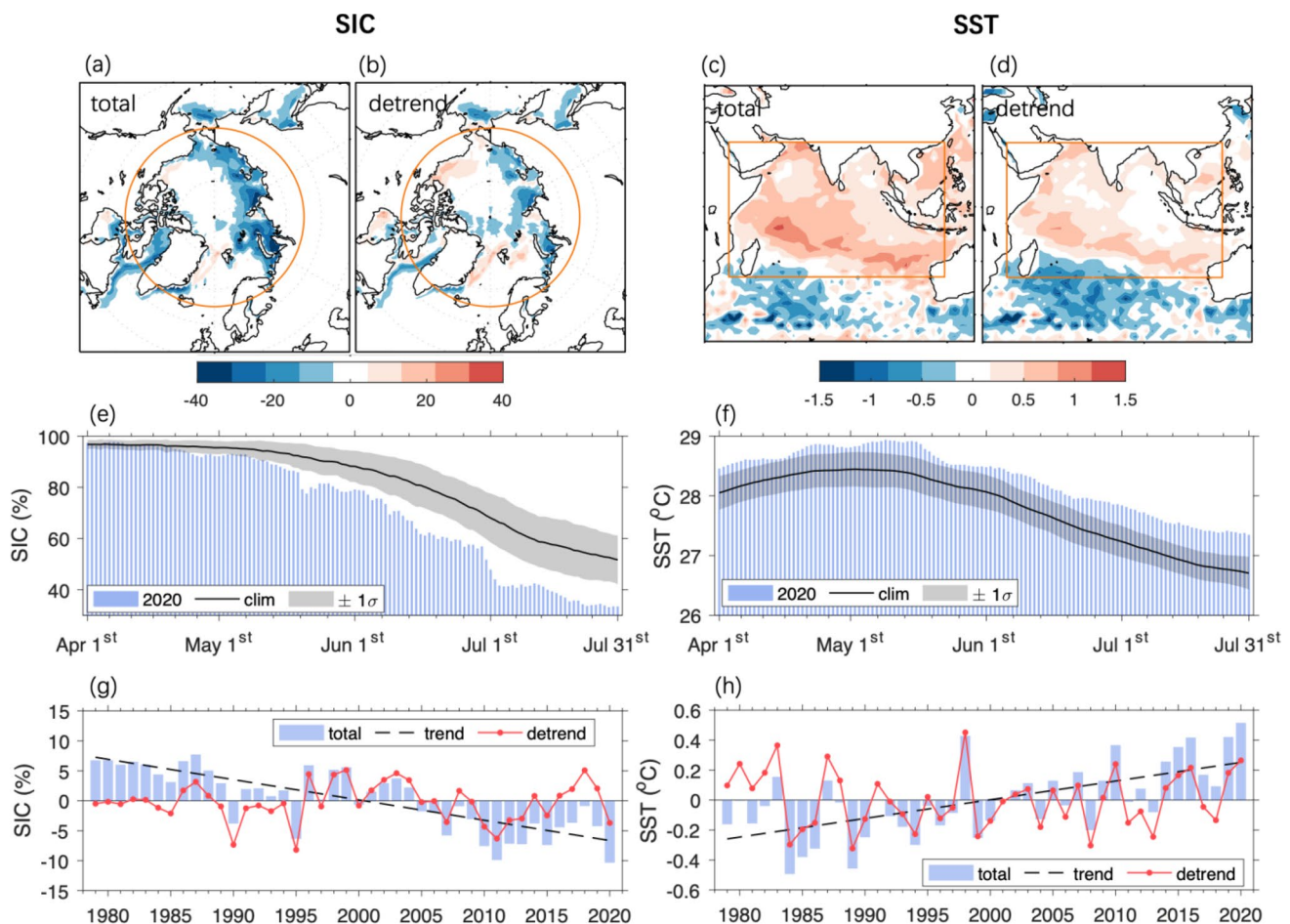


Fig. 2 **a–d** Anomalies of SIC (%) and SST (°C) averaged from May through July in 2020, with total anomalies in panels **a** and **c** and detrended anomalies in panels **b** and **d**. Only significant anomalies are shaded. The orange lines highlight the Arctic and IO regions we used to force the CAM6 simulations (see details in Sect. 2). **e–f** The daily evolution of SIC and SST (blue bars) averaged over the Arctic region north of Siberia (65°–90° N, 60°–180° E) and over IO (25° S–25° N, 40°–120° E), respectively, from April 1st to July

31st in 2020, comparing with their climatology (black lines). The grey shadings denote the range of ± 1 standard deviation of interannual variability. **g–h** April–July averaged SIC and SST anomalies over the Arctic region north of Siberia and IO, respectively, from 1979 to 2020 (blue bars). The black dashed line represents the long-term trend and the red solid line represents the detrended anomalies. Results for individual calendar months from April to July are generally similar

western North Pacific, enhancing the East Asian Westerly jet that supplies excessive moisture into the Meiyu-Baiu region (Zhou et al. 2021).

The effects of other tropical oceans in the 2020 Meiyu-Baiu rainfall have also been studied, but they are significantly weaker than the effect of IO warming. The weak central Pacific El Niño-like warming in 2019/2020 winter rapidly decayed, leading to a weaker La Niña-like cooling in the early summer of 2020 (Pan et al. 2021). In response to the cool SST in the tropical central-eastern Pacific (CEP) in summer 2020, numerical models simulate an anomalous western North Pacific anticyclone (WNPAC) as expected from the Gill response, but the WNPAC is much weaker than that caused by the IO warming (Pan et al. 2021; Tang et al. 2021). A warm tropical western Pacific (WP) in June–July

2020 generates an anomalous western North Pacific cyclone (WNPC) in atmospheric circulation simulations, which is opposite to the observations, suggesting that the warm WP is not a cause but a consequence of the atmospheric circulation anomalies (Ueda et al. 2021). The tropical Atlantic is also warmer than usual in June–July 2020, but its impact is less pronounced compared with the influence of IO and CEP and inconsistent between models (Pan et al. 2021; Tang et al. 2021). IO warming is therefore considered to be the primary contributor to the extreme Meiyu-Baiu rainfall in 2020.

However, Zhou et al. (2021) found that the IO warming led to suppressed precipitation over the Meiyu-Baiu region in July in model simulations, which is opposite to the observation. Although they suggested that this may stem from the model bias in the East Asian Westerly jets in July, this

result challenges the importance of IO warming in driving the Meiyu-Baiu rainfall in July 2020.

In early June 2020, the Arctic sea-ice extent in the Laptev Sea dropped to its lowest level for the same time of year since 1979 (NSIDC 2020a). In fact, the Arctic sea ice retreated considerably faster from the Siberian coast than usual from late April 2020 (Fig. 2a, e) due to an extraordinary Russian heatwave lasting from January to June (NSIDC 2020a; b; Overland and Wang 2020), which combines internal variations and anthropogenic warming (Ciavarella et al. 2020). Superimposed on a long-term decline trend due to global warming, the Arctic sea ice concentration (SIC) in late spring-early summer along the Siberian coast exhibits substantial interannual fluctuations due to the internal variability (Fig. 2g). In 2020, the contributions from the long-term trend and interannual fluctuations are comparable (Fig. 2g). Our recent study shows that the extremely low Arctic sea ice in the late spring and early summer of 2020 also contributed to the heavy Meiyu-Baiu rainfall in 2020 (Chen et al. 2021). We found that the early retreat of Arctic sea ice created more open waters along the Siberian coast in late spring 2020, which absorbed extra sunlight and released more longwave radiations and turbulent heat flux into the above atmosphere in early summer, resulting in a zonally-originated warming belt along the Siberian coast. The warmer Arctic reduced the Asian polar-front jet by weakening the meridional temperature gradient and local baroclinicity. As a result, more frequent atmospheric blockings occurred in Northeast Asia, which brought cold air into the Meiyu-Baiu region, disrupting the seasonal march of the summer monsoon and anchoring the Meiyu-Baiu front. In an atmosphere model experiment forced by the Arctic SIC and SST in 2020, we found that the precipitation is increased over the Meiyu-Baiu region, especially in July. Many observational and modeling studies have proved that the Arctic sea ice changes could alter the atmospheric teleconnections across Eurasia, thereby affecting the precipitation over East Asia in spring and summer (e.g., Wu et al. 2009, 2016; He et al. 2018). Though the Arctic sea-ice loss in the warm season has a humbler influence on atmospheric circulations relative to that in the cold season (Dai et al. 2019), its influence is still notable on the polar-front jet and the waves embedded in it (Coumou et al. 2018). Our previous study explained how the reduced Arctic sea ice in late spring and early summer 2020 alters the atmospheric circulation in Northeast Asian high latitudes and thus the Meiyu-Baiu rainfall (Chen et al. 2021), but the relative importance of Arctic sea-ice loss and IO warming remains unclear.

In this study, we investigate the atmospheric circulation characteristics responsible for the enhanced Meiyu-Baiu rainfall in June and July 2020 using reanalysis data, and we further investigate how the Arctic sea-ice loss and IO warming may influence these circulation characteristics and

thus precipitation with the aid of the atmospheric general circulation model (AGCM) simulations. In particular, we focus on the following questions: (1) In June and July 2020, which atmospheric circulation anomalies directly enhance the Meiyu-Baiu rainfall? (2) By affecting these primary circulation anomalies, whether and how does the Arctic sea-ice loss and IO warming affect the Meiyu-Baiu rainfall? (3) And what is the relative importance of the Arctic sea-ice loss and IO warming? The answers may help us better explain the unusual Meiyu-Baiu rainfall in 2020 (especially in July) and gain a deeper understanding of the combined effects of the Arctic and tropic oceans on the mid-latitude extreme weather.

This paper proceeds as follows. Section 2 describes the data and model experiments. Using reanalysis data, Sect. 3 investigates the atmospheric circulation characteristics responsible for the anomalous moisture supply and ascending motion over the Meiyu-Baiu region in June and July 2020. A set of AGCM experiments in Sect. 4 examines how the Arctic sea-ice loss and IO warming affect the atmospheric circulation characteristics directly responsible for the enhanced Meiyu-Baiu rainfall. The final section includes a summary and discussions.

2 Data and method

2.1 Reanalysis data

Monthly data on precipitation, geopotential height, air temperature, specific humidity, vertical velocity, zonal and meridional winds were obtained from ERA5 reanalysis (Hersbach et al. 2020) provided by the European Center for Medium-Range Weather Forecasts (ECMWF). The data is on a $1^\circ \times 1^\circ$ horizontal grid, spanning from January 1979 to July 2020. The precipitation of ERA5 over the middle and lower reaches of the Yangtze River in June–July 2020 was validated using a dataset combining observations from rain gauges, radars and satellite sensors (Chen et al. 2021). All anomalies are defined relative to the daily climatology averaged from 1979 to 2020. A significant anomaly is defined at the 5% level based on a Student's *t*-test.

2.2 Moisture budget

Following Seager and Henderson (2013), we used a flux form moisture equation in a *p* coordinate that is vertically integrated from the near-surface pressure p_s to the top of the atmosphere:

$$P - E = -\frac{1}{g\rho} \int_0^{p_s} \frac{\partial q}{\partial t} dp - \frac{1}{g\rho} \int_0^{p_s} \nabla_h \cdot (\vec{V}q) dp - \frac{1}{g\rho} (\omega_s q_s), \quad (1)$$

where P is the precipitation, E is the evaporation, q is the specific humidity, \vec{V} is the horizontal velocity vector, g is the gravity acceleration, ρ is the water density, and the subscript s denotes the near-surface variables. The 100 hPa level is assumed to be the top of the atmosphere since the specific humidity is close to zero there, and the 1000 hPa level is assumed to be the near-surface level. These approximations are validated by a closed test given in Sect. 3. For monthly mean, the local tendency term is negligible. The monthly mean precipitation anomaly can be derived:

$$P' = E' - \frac{1}{g\rho} \left\langle \nabla_h \cdot (\vec{V}q) \right\rangle' - \frac{1}{g\rho} (\omega_s q_s)', \quad (2)$$

where the prime denotes the monthly-mean deviation from the climatology and the angle bracket $\langle \dots \rangle = \int_{1000\text{hPa}}^{100\text{hPa}} \dots dp$ represents a vertically integrated from 1000 to 100 hPa.

2.3 Model experiments

We performed numerical experiments using an updated atmospheric model, the Community Atmosphere Model version 6 (CAM6) (Danabasoglu et al. 2020). The CAM6 was run with a $1.25^\circ\text{lon} \times 0.9^\circ\text{lat}$ horizontal resolution and 32 levels from the surface to 2.26 hPa. The climatological SST and SIC averaged over 1995–2005 were used in the control experiment (CTL). The CTL experiment was continuously run for 50 years after a 25-year spin-up. Besides the CTL experiments, we conducted four perturbation experiments running from April 1st to July 31st. In the first perturbation experiment (GLOBAL), we prescribed the global SST and Arctic SIC in 2020. The global SST anomalies in 2020 can be found in many previous studies (e.g., Liang et al. 2021; Pan et al. 2021), and the Arctic SIC anomalies in 2020 are shown in Fig. 2a. The second perturbation experiment (IO) is the same as CTL but uses 2020 SST only in the tropical IO (25°S – 25°N , 40° – 120°E). The spatial distribution and temporal variations of the IO SST are shown in Fig. 2c and f. Following Zhou et al. (2021), the South China Sea was included in this domain to reduce the artificial temperature contrast between IO and WP, which may fabricate atmospheric circulation responses. The third perturbation experiment (ARCTIC) is the same as CTL but used 2020 SST and 2020 SIC north of 65°N . The spatial distribution and temporal variations of the Arctic SIC in 2020 can be found in Fig. 2a and e. The negative SIC anomaly in early

summer 2020 is mainly along the Siberian coast, including the Kara Sea, Laptev Sea, and East Siberian Sea (Fig. 2a). The fourth experiment (IO&ARCTIC) is the same as CTL but used 2020 SST and SIC north of 65°N and 2020 SST in tropical IO. Each perturbation experiment has 20 members initialized from slightly different atmospheric temperature conditions. The ensemble-mean difference of perturbation experiment minus CTL experiment was defined as the response. A significant response was defined at the 10% level based on a Student's t -test.

3 Factors directly contributing to enhanced Meiyu-Baiu rainfall in June and July of 2020

Precipitation occurs when water vapor condenses in the ascending air. To identify the primary atmospheric dynamical and thermodynamic factors directly responsible for the enhanced Meiyu-Baiu rainfall region in June and July 2020, we perform a moisture budget analysis to investigate the causes of abundant moisture supply, and then we use the mid-troposphere temperature advection to understand the ascending anomalies. In Sect. 4, the primary factors identified in this section will be used to connect the prescribed IO warming and Arctic sea-ice loss to the precipitation response in CAM6 simulations.

3.1 Moisture budget

Figure 3 shows the monthly-mean anomalies of precipitation, evaporation, horizontal and vertical convergence of moisture around the Meiyu-Baiu region in June and July 2020. As expected from Eq. (2), the domain-averaged precipitation anomalies are nearly balanced by the other three terms (Fig. 3). A slight discrepancy exists likely due to the local tendency of humidity. It is found that the enhanced precipitation is primarily caused by horizontal convergence of moisture (Fig. 3c, g). It accounts for 84% (70%) of the extra precipitation over the Meiyu-Baiu region in June (July). The contribution from surface evaporation is negligible (Fig. 3b, f). The vertical convergence of moisture accounts for only 11% of the enhanced precipitation over the Meiyu-Baiu region in June (Fig. 3d), but this proportion increases to 20% in July (Fig. 3h). Due to the coupling between moisture vertical transport and precipitation, the precise contribution of vertical moisture convergence on enhanced precipitation cannot be determined. Despite that, we can still infer an increasing importance of vertical motions from June to July.

Horizontal convergence of moisture, the primary contributor to the enhanced precipitation over the Meiyu-Baiu

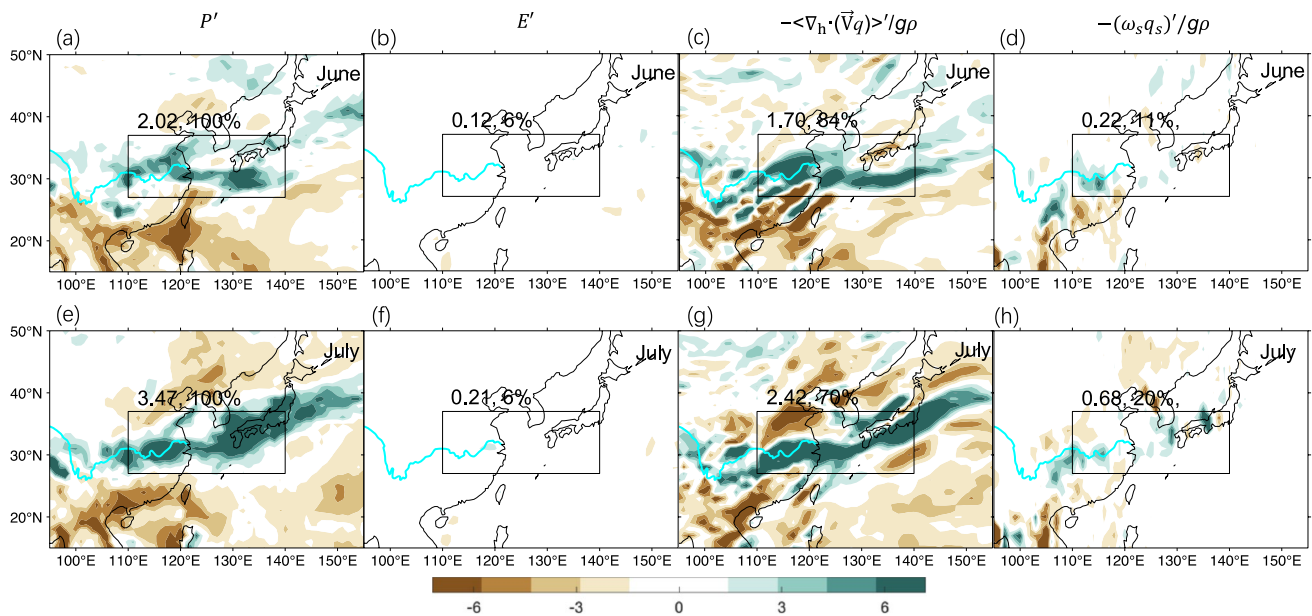


Fig. 3 Monthly mean anomalies (mm day^{-1}) of **a, e** precipitation (P'), **b, f** evaporation (E'), vertical integrated **c, g** horizontal moisture convergence $-\langle \nabla_h \cdot (\bar{\mathbf{v}}q) \rangle / g\rho$ and **d, h** vertical moisture conver-

gence $-(\omega_s q_s)' / g\rho$ in (upper) June and (lower) July 2020. The black box highlights the Meiyu-Baiu region. The domain-averaged value over the Meiyu-Baiu region and its ratio (in %) to the domain-averaged precipitation anomaly are given at the top of the box

region in June–July 2020, can be broken down into three terms:

$$\langle \nabla_h \cdot (\bar{\mathbf{v}}q) \rangle' = \langle \nabla_h \cdot (\bar{\mathbf{v}}_b q') \rangle + \langle \nabla_h \cdot (\bar{\mathbf{v}}' q_b) \rangle + \langle \nabla_h \cdot (\bar{\mathbf{v}}' q') \rangle, \quad (3)$$

where the subscript b denotes background state defined as the 1979–2020 climatology. The right-hand side terms of Eq. (3) represent the horizontal moisture convergence due to humidity anomalies, horizontal wind anomalies, and their combined effect, respectively. As shown in Fig. 4, the distribution and magnitude of the anomalous horizontal moisture convergence are mainly attributed to the dynamical effect from horizontal circulation anomalies (Fig. 4a, d). Although the thermodynamic effect (Fig. 4b, e) and nonlinear effect (Fig. 4c, f) also contribute positively to the west–east structure of the rain belt, their total contributions averaged over the Meiyu-Baiu region are less than 20%.

We further divide the horizontal moisture convergence due to horizontal wind anomalies $-\langle \nabla_h \cdot (\bar{\mathbf{v}}' q_b) \rangle$ into two components: $-\langle q_b \nabla_h \cdot \bar{\mathbf{v}}' \rangle$, representing the effect of convergent circulation anomalies on the background humidity, and $-\langle \bar{\mathbf{v}}' \cdot \nabla_h q_b \rangle$, representing the background humidity advected by the circulation anomalies. It is found that the effect of horizontal convergence anomalies generally reproduces the effect from the total horizontal circulation

anomalies (compare Fig. 4a, d to Fig. 5a, c), while the effect of horizontal advection is less evident (Fig. 5b, d).

A closer investigation suggested that the moisture converged by anomalous horizontal wind convergence results from the meridional wind anomalies (Fig. 6), particularly pronounced in July (Fig. 6b, d). Northerly anomalies from the higher latitudes and southerly anomalies from the lower latitudes result in a zonally-originated convergence belt over the Meiyu-Baiu region (Fig. 7a, b). This meridional wind convergence is efficient in moisture convergence because the background specific humidity over East Asia generally decreases along the latitude northward (contours in Fig. 7c). The southerly anomalies bring moisture across the isohygrometric lines into the Meiyu-Baiu region, and the northerly anomalies prevent moisture from traveling further north. By contrast, the westerly anomalies around the Meiyu-Baiu region during June and July 2020 (Ding et al. 2021; Li et al. 2021; Zhou et al. 2021) generate a moisture divergence (Fig. 6a, c) due to the background specific humidity decreasing from southeastern China to the western North Pacific (Fig. 7c).

To sum up, the enhanced Meiyu-Baiu rainfall in June–July 2020 is dynamically driven. More specifically, the moisture is concentrated by the anomalous meridional wind convergence, which is particularly evident in July. The thermodynamic effect from humidity anomalies is relatively weak and decreases from June to July (Fig. 4b,

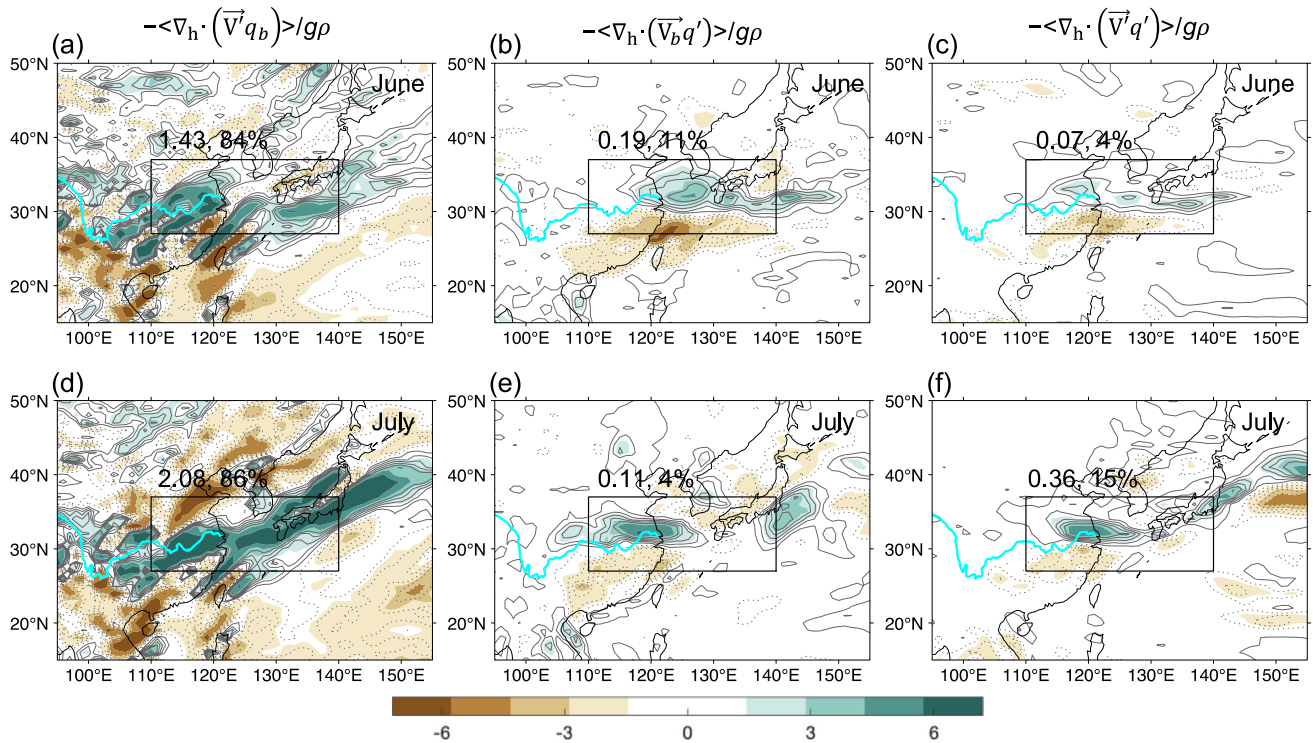


Fig. 4 Monthly mean anomalies (mm day⁻¹) of vertical integrated horizontal moisture convergence due to **a, d** circulation anomalies ($-\langle \nabla_h \cdot (\bar{\mathbf{V}}^T q_b) \rangle / g\rho$), **b, e** specific humidity anomalies ($-\langle \nabla_h \cdot (\bar{\mathbf{V}}_b q') \rangle / g\rho$), and **c, f** both of them ($-\langle \nabla_h \cdot (\bar{\mathbf{V}}^T q') \rangle / g\rho$)

in (upper) June and (lower) July 2020. The black box highlights the Meiyu-Baiu region. The domain-averaged value over the Meiyu-Baiu region and its ratio (in %) to the domain-averaged value of total vertical integrated horizontal moisture convergence are given at the top of the box

Fig. 5 Anomalies (mm day⁻¹) of vertical integrated horizontal moisture convergence due to circulation anomalies ($-\langle \nabla_h \cdot (\bar{\mathbf{V}}^T q_b) \rangle / g\rho$) is split into two components caused by **a, c** anomalous convergence of background humidity ($-\langle q_b \nabla_h \cdot \bar{\mathbf{V}}^T \rangle / g\rho$) and **b, d** anomalous advection of background humidity gradient ($-\langle \bar{\mathbf{V}}^T \cdot \nabla_h q_b \rangle / g\rho$), respectively, in (upper) June and (lower) July 2020. The black box highlights the Meiyu-Baiu region. The domain-averaged value over the Meiyu-Baiu region is given at the top of each box

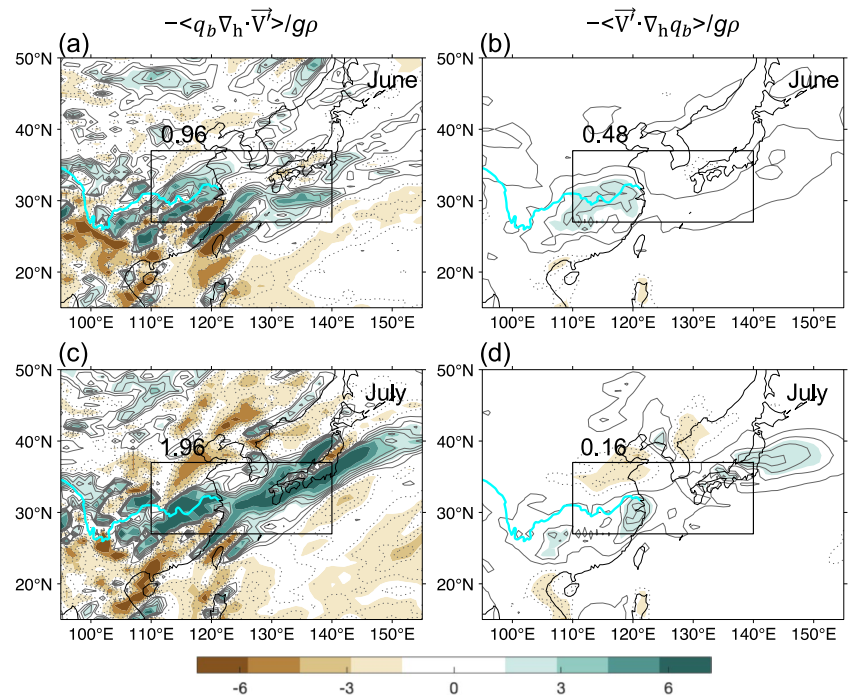


Fig. 6 Anomalies of vertical integrated horizontal moisture convergence due to anomalous horizontal convergence ($-\langle q_b \nabla_h \cdot \bar{\mathbf{V}}' \rangle / g\rho$) is split into the **a, c** zonal component ($-\langle q_b \partial u' / \partial x \rangle / g\rho$) and **b, d** meridional component ($-\langle q_b \partial v' / \partial y \rangle / g\rho$). The monthly mean results (mm day^{-1}) are shown for (upper) June and (lower) July 2020. The black box highlights the Meiyu-Baiu region

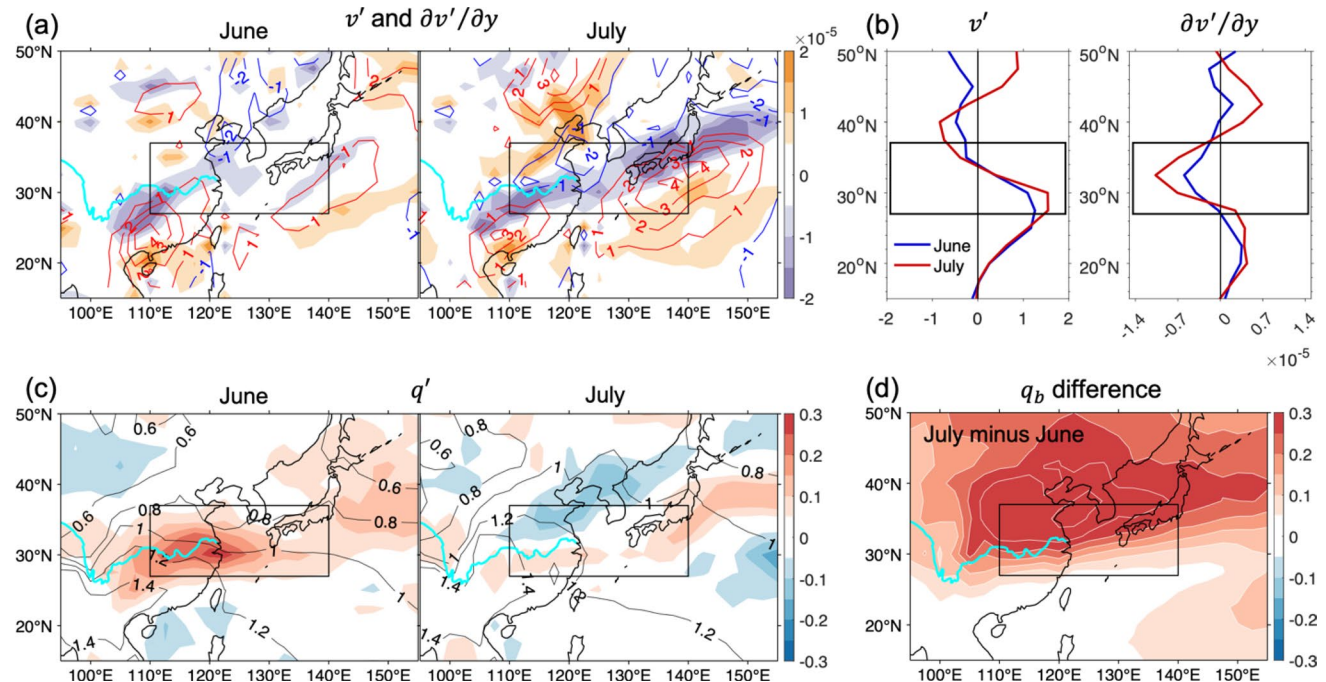
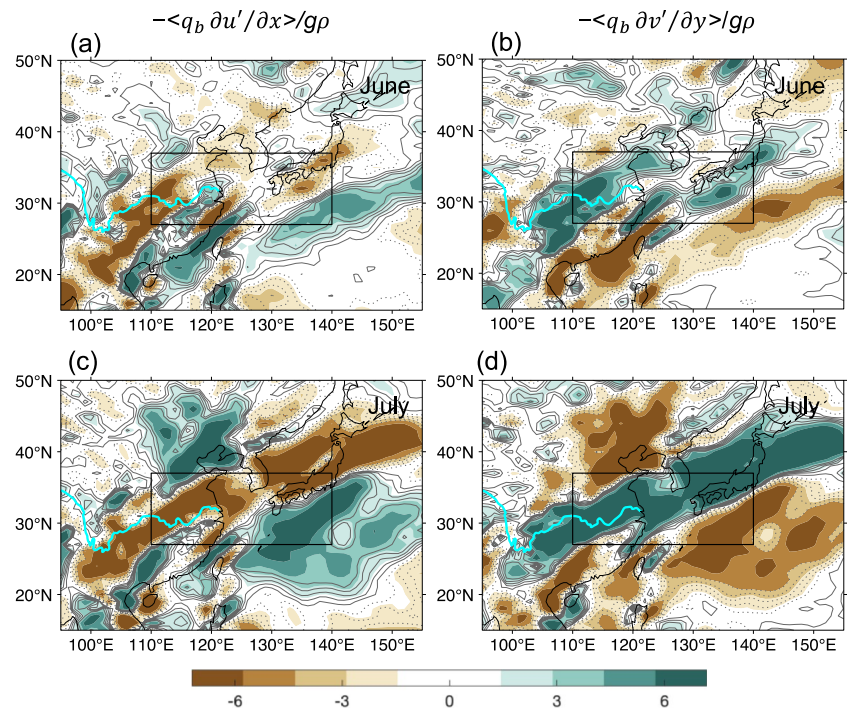


Fig. 7 **a** Monthly mean 850 hPa meridional wind anomalies (v' ; contours; interval = 1 m s^{-1}) and their meridional gradient ($\partial v' / \partial y$; shading; s^{-1}) in June and July 2020, and **b** their zonally-averaged results within the longitudinal range of the Meiyu-Baiu region. **c** Monthly mean 850 hPa specific humidity anomaly (shading; kg kg^{-1}) in June

and July 2020 and its climatology (contours; interval = 0.2 kg kg^{-1}). **d** Difference of the climatological specific humidity between July and June (kg kg^{-1}). The black box highlights the Meiyu-Baiu region or its latitude range

e). In fact, the specific humidity anomaly over the Meiyu-Baiu region was very weak in July 2020 (Fig. 7c), while the background specific humidity over East China in July

is significantly larger than that in June (Fig. 7d). Thus, the excessive moisture supply for the particularly heavy Meiyu-Baiu rainfall in July 2020 is mainly caused by the

abundant background moisture converged by convergent meridional winds. Wang et al. (2021) have divided the water vapor convergence during the entire 2020 Meiyu-Baiu season into three components in a similar manner to Eq. (3) and confirmed that the circulation anomalies contributed more than humidity anomalies, but they conjectured that the anomalous strong East Asian summer monsoon is responsible for the circulation anomalies. Our elaborate decomposition indicates that both southerly and northerly anomalies are crucial, despite the fact that the latter's causes are not well understood.

3.2 Ascending motions

As indicated by Sampe and Xie (2010), the ascending motions of Meiyu-Baiu rainfall are mainly induced adiabatically by the warm advection tied to East Asian Westerly jet, and it is further amplified and sustained by the resultant condensational heating. This mechanism has been used to explain the seasonal march (Sampe and Xie 2010), inter-annual variations (Kosaka et al. 2011), and extreme cases (Zhou et al. 2021) of Meiyu-Baiu rainfall. Following these studies, we examine the horizontal temperature advection anomaly pattern and compare it with the vertical velocity anomalies in the middle troposphere (Fig. 8a, b). Their vertical profiles averaged over the Meiyu-Baiu region through the troposphere are also examined (Fig. 8f, g). In June and July 2020, warm advection over the Meiyu-Baiu region is found at 500 hPa (shading in Fig. 8a, b) and through the troposphere (Fig. 8f), which coincides well with the ascending motions over the Meiyu-Baiu region (contours in Fig. 8a, b). The warm advection and upward motions are more prominent and concentrated in July than in June (Fig. 8a, b), corresponding to the heavier precipitation in July (Fig. 3e). The zonal temperature advection anomalies (Fig. 8c, d) broadly resemble the total horizontal temperature advection anomalies (Fig. 8a, b) in both distribution and magnitude, suggesting that the warm advection over the Meiyu-Baiu region is dominated by zonal temperature advection. This is due to the enhanced East Asian Westerly jets in June and July 2020 (Figs. 1a and 8e) as well as the large thermal contrast from the warm Tibetan Plateau to the cold North Pacific in summer caused by the different warming rates over land (especially at high altitudes) and ocean (Okada and Yamazaki 2012; Dai et al. 2013). Note that the westerly anomalies over the Meiyu-Baiu region are restricted in the lower troposphere in June (Fig. 8e); in contrast, the westerly in July are ~ 1.2 standard deviations (STD) above the climatology, with a quasi-barotropic vertical structure through the troposphere (Fig. 8e). The westerly anomalies in the mid-to-high troposphere are likely more effective in temperature advection because the zonal thermal contrast over East Asia is greater in the mid-upper troposphere than in the lower

troposphere (Dai et al. 2013). Accordingly, the warm advection averaged over the Meiyu-Baiu region is above one STD than the climatology in July but within ± 1 STD range in June (Fig. 8f). The ascending motion over the Meiyu-Baiu region is therefore more pronounced in the mid-upper troposphere in July (Fig. 8g).

Ascending anomalies may also result from a strengthening westerly jet in the upper levels (Chen and Zhai 2014; Ding et al. 2021). When the westerly jet strengthens, air parcels are accelerated in the entrance region along the jet axis, causing ageostrophic southerlies across the jet axis in the jet entrance and resulting in upper-level divergence and ascending motions in the south. However, the association between strengthened westerlies and ascending motions goes both ways: a strengthening westerly can also result from anomalous ascending motions. In June 2020, as the enhanced westerlies prevail only in the lower troposphere (Fig. 8e), we find no significant divergence in the upper troposphere. In July 2020, westerly anomalies extend into the upper troposphere (Fig. 8e), but the upper-level divergence appears to be located east of ascending anomalies rather than south of the jet axis (not shown). It seems that upward motions drive divergent flow in the upper troposphere, reinforcing westerlies in the east. In other words, the upper-level divergence in July 2020 is more likely a consequence than a cause of the ascending anomalies.

So far, this section has identified two primary atmospheric circulation characteristics responsible for the enhanced Meiyu-Baiu rainfall in June and July 2020. First, anomalous northerlies and southerlies converge along the Meiyu-Baiu region, dynamically generating moisture convergence. Secondly, enhanced westerly jets promote ascending motions via warm advection in the middle troposphere. The southerly anomalies are associated with an anomalous WNPAC, and the northerly anomalies seem to be associated with a dipole pattern in Northeast Asia with an anticyclone in the north and a cyclone in the south (Fig. 9a, b, d, e). The westerly anomalies are also related to the anomalous WNPAC and dipole pattern in Northeast Asia (Fig. 9a, b, d, e). Noted that the anomalous WNPAC tilted northward in June (Fig. 9c), constraining westerly anomalies in the lower troposphere (Fig. 8e), while it became quasi-barotropic in July (Fig. 9f), allowing the zonal winds to increase through the troposphere (Fig. 8e). Thus, the Meiyu-Baiu rainfall is particularly strong in July, not only because of the stronger meridional convergence in July (Fig. 7b) but also because of the stronger mid-upper tropospheric westerly jets (Fig. 8e) associated with the barotropic circulation anomalies in July (Fig. 9f).

Some previous studies suggested that IO warming and Arctic sea-ice loss are likely responsible for similar large-scale atmospheric circulation characteristics. A warm IO can result in an anomalous WNPAC via the

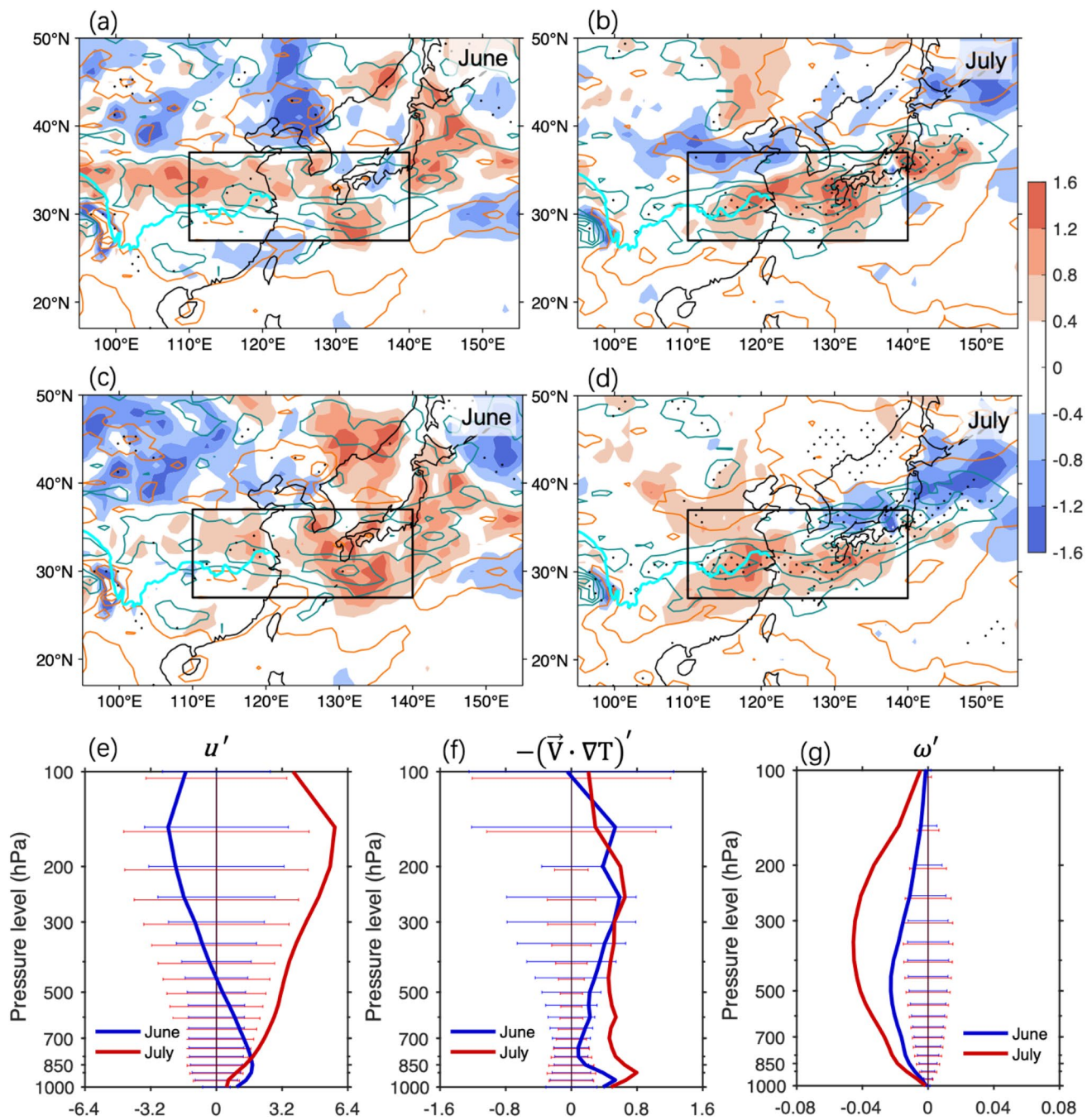


Fig. 8 **a–d** Monthly-mean anomalies of 500 hPa vertical velocity (ω' ; contours; interval = 0.04 Pa s^{-1}) in (left) June and (right) July 2020, corresponding with **a**, **b** horizontal temperature advection anomalies ($-(\vec{V} \cdot \nabla T)'$) and **c**, **d** zonal temperature advection anomalies ($-(u\partial T/\partial x)'$; shading; 10^{-5} K s^{-1}) at 500 hPa. The black box highlights the Meiyu-Baiu region. The stippling indicates the signifi-

cant anomaly. **e–g** Vertical profiles of domain-averaged anomalies of **e** zonal wind (u' ; m s^{-1}), **f** horizontal temperature advection ($-(\vec{V} \cdot \nabla T)'$; K s^{-1} per 100 km), and **g** vertical velocity (ω' ; Pa s^{-1}) over the Meiyu-Baiu region in June and July 2020. The horizontal line denotes the range of ± 1 standard deviation

Indo-western Pacific Ocean capacitor (Zhou et al. 2021). Arctic sea-ice loss favors anomalous high pressure in Northeast Asia (Chen et al. 2021), which weakens westerlies along its south flank and creates cyclonic shear

(negative anomalies in du/dy), leading to a dipole pattern in Northeast Asia. The dipole pattern in Northeast Asia also may result from the Pacific-Japan (PJ) teleconnection triggered by the tropical convection (Nitta 1987;

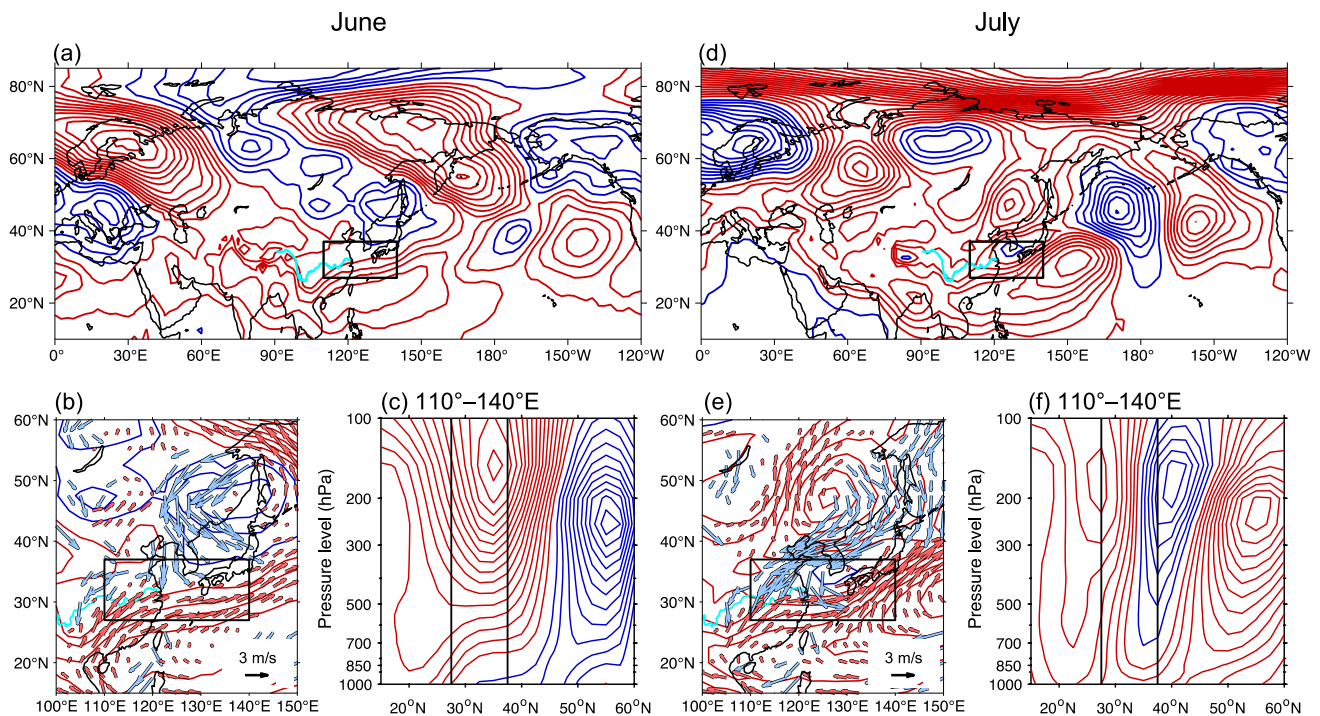


Fig. 9 **a** Monthly-mean 850 hPa geopotential height anomalies (contours, interval=50 gpm) over Eurasia in June 2020, red lines for positive and blue lines for negative values. **b** Monthly-mean 850 hPa geopotential height anomalies (contours) and horizontal winds (vectors; with red for southerlies and blue for northerlies) around the

Meiyu-Baiu region in June 2020. **c** Latitude-pressure cross section of the zonal-averaged geopotential height anomaly over the Meiyu-Baiu region (contours, interval=50 gpm), with red lines for positive and blue lines for negative values. **d–f** is similar to **a–c** but for July 2020. The black box highlights the Meiyu-Baiu region or its latitude range

Huang 1992). Nevertheless, it remains unknown whether and how the meridional convergence and mid-troposphere westerly anomalies in June and July 2020 are related to the IO warming and Arctic sea-ice loss. To address this question, we turn to model simulations in the next section to isolate the effects of IO warming and Arctic sea-ice loss.

4 Effects of IO warming and Arctic sea-ice loss

Figure 10 shows the monthly-mean responses of precipitation and 850 hPa geopotential height for each CAM6 experiment in June and July. In general, the GLOBAL experiment reproduces the precipitation anomaly pattern in June (Fig. 10a) but misses the particularly heavy precipitation in July (Fig. 10e). This is likely due to the prescribed warm SST in tropical WP and western North Pacific in the GLOBAL experiment, which ought to be a consequence of atmospheric circulation response rather than a driver. Warm SSTs in the WP and western North Pacific could trigger a cyclone anomaly over the western North Pacific, thereby artificially offsetting the anomalous WNPAC caused by IO warming (Guo et al. 2021; Ueda et al. 2021). The

IO&ARCTIC experiment better represents the observed circulation anomalies and enhanced precipitation in the Meiyu-Baiu region (Fig. 10b, f). Importantly, it captures the exceptionally heavy precipitation in July, allowing us to analyze the role played by IO and Arctic in the atmospheric and precipitation anomalies in July.

In June, the IO experiment simulates enhanced precipitation over the Meiyu-Baiu region and a PJ-like pattern with alternating negative and positive geopotential height centers extending from the Philippines to Northeast Asia (Fig. 10c). Many studies have demonstrated how IO warming generates the PJ teleconnection (e.g., Yang et al. 2007; Xie et al. 2009; Chowdary et al. 2011). IO warming could induce Kelvin waves propagating eastward near the equator, leading to an anomalous anticyclonic circulation over the Philippines. Consequently, suppressed convection activity generates a meridional-propagating wave train along the east coast of Asia. Meanwhile, the atmospheric circulation response in the ARCTIC experiment exhibits a zonally-originated wave train across the Eurasian high latitudes with a positive geopotential height center in Northeast Asia (Fig. 10d). The wave train pattern is similar to the regressed pattern on reducing summer sea-ice extent (Tang et al. 2014), which indicates it is likely to be a response to the Arctic sea-ice loss in summer. Likewise, in large ensemble experiments

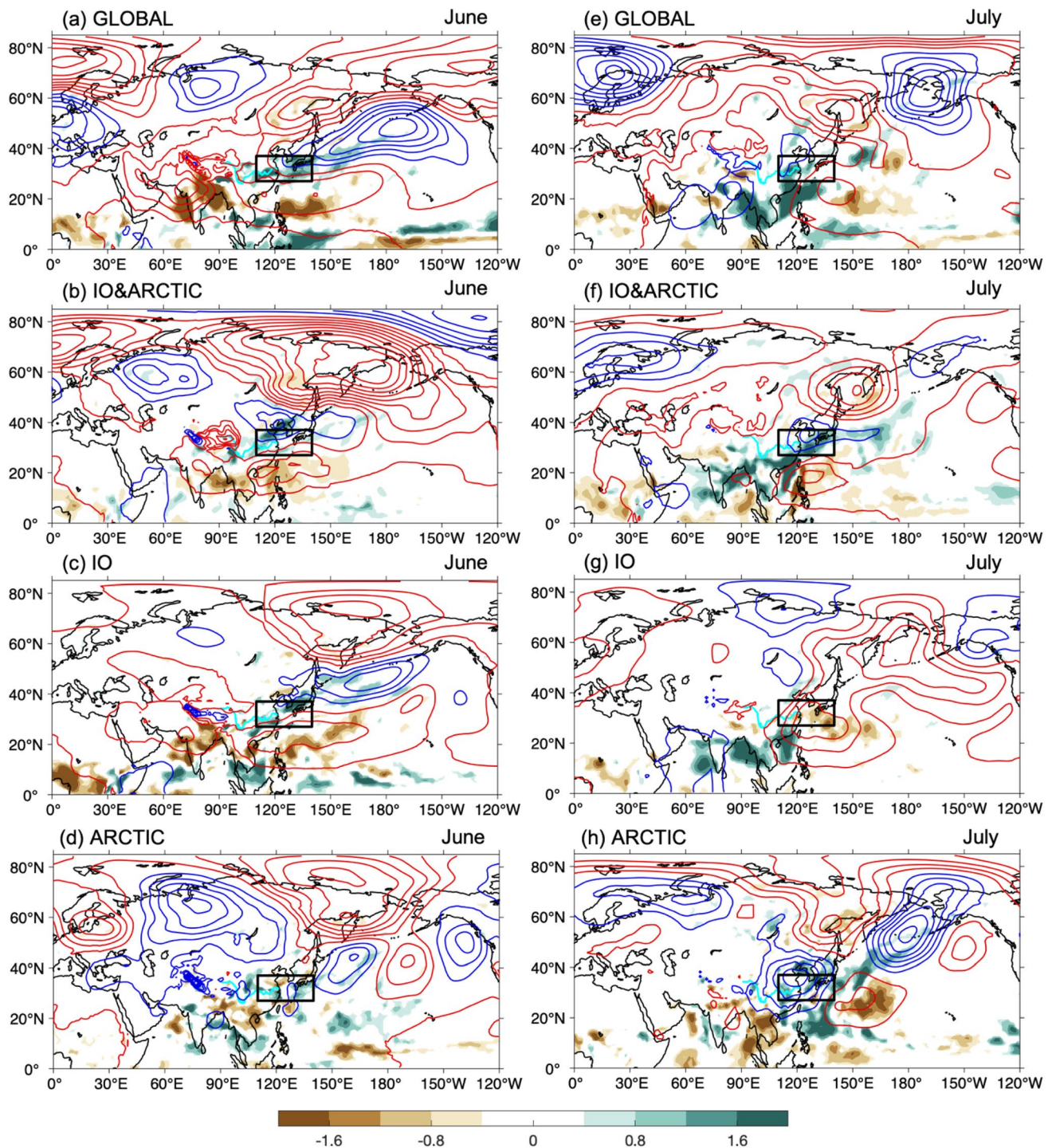


Fig. 10 Responses of 850 hPa geopotential height (contours, interval=4 gpm; with red lines for positive values and blue lines for negative values) and precipitation rate (shading; mm day⁻¹) from **a**,

e GLOBAL, **b**, **f** IO & ARCTIC, **c**, **g** IO, and **d**, **h** ARCTIC experiments in (left) June and (right) July. Only significant responses are shaded. The black box highlights the Meiyu-Baiu region

forced by Arctic sea-ice loss, Streffing et al. (2021) found a significant increase in blocking highs over Scandinavia and Northeast Asia. As the Arctic sea ice retreats from the north coast of Eurasian, extensive open-water areas occur, which

absorb more solar radiation and warm the air above. The resultant change in meridional gradient of temperature and baroclinicity modify the polar-front jet and eddy forcing, amplifying the quasi-stationary wave trains embedded in

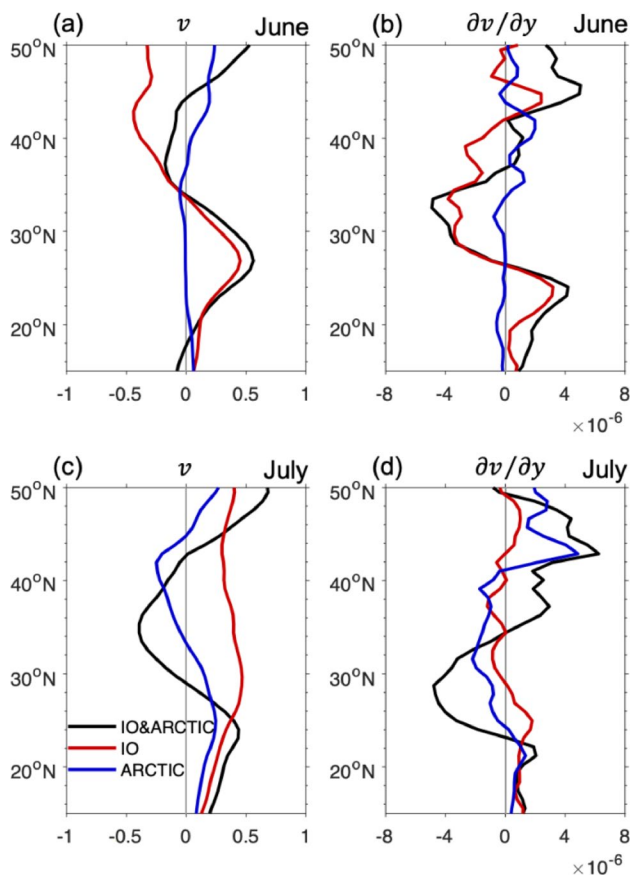


Fig. 11 Responses of 850 hPa (left) meridional winds (m s^{-1}) and (right) their meridional gradient (s^{-1}) from IO&ARCTIC (black line), IO (red line), and ARCTIC (blue line) experiments in (upper) June and (bottom) July

the polar-front jet and resulting in a “two ridges and one trough” pattern (Coumou et al. 2018; Zhang et al. 2021). In the ARCTIC experiment, the precipitation response in June is much weaker than that in the IO experiments (Fig. 10c, d). Averaged over the Meiyu-Baiu region, the precipitation anomalies caused by Arctic sea-ice loss are only $\sim 35\%$ of that caused by IO warming. Therefore, although both IO warming and Arctic sea-ice loss are responsible for the large-scale atmospheric circulation anomalies in June, IO warming accounts for most precipitation anomalies in June.

Figure 11 illustrates the responses of meridional winds and their gradient averaged over the longitudinal range of the Meiyu-Baiu region in IO&ARCTIC, IO, and ARCTIC experiments. The IO&ARCTIC and IO experiments show a substantial meridional convergence over the Meiyu-Baiu latitudes in June, while it is unclear for the ARCTIC experiment (Fig. 11b). The convergence is jointly caused by the southerlies anomalies due to the anomalous WNPAC and the northerlies anomalies due to the anomalous Northeast Asian cyclone (Figs. 10b and 11b). Thus, the meridional convergence response in June is primarily attributed to the

IO warming and the associated PJ teleconnection pattern (Fig. 10c), rather than the Arctic sea-ice loss and the associated high-latitude wave train pattern (Fig. 10d).

Figure 12 exhibits the responses of mid-troposphere vertical velocity, horizontal winds and zonal temperature advection in the IO&ARCTIC, IO, and ARCTIC experiments. The vertical velocity response pattern is broadly consistent with the precipitation response (compare Fig. 10 to Fig. 12). In June, an enhanced westerly over the Meiyu-Baiu region is found in the IO&ARCTIC and IO experiments (Fig. 12a, b) but not in the ARCTIC experiment (Fig. 12c). In the IO&ARCTIC and IO experiments, the anomalous westerly winds lead to strong warm advection in the middle troposphere over the Meiyu-Baiu region, which promotes ascending anomalies (Fig. 12a, b). The ascent response in the ARCTIC experiment is rather weak in June (Fig. 12c), consistent with its weaker precipitation response (Fig. 10d). Thus, the ascent response over the Meiyu-Baiu region in June is also primarily due to the IO warming.

Therefore, despite the Arctic sea-ice loss accounting for the large-scale atmospheric circulation anomalies over the Eurasian high latitudes in June 2020, the IO warming is responsible for most of the Meiyu-Baiu rainfall anomalies in June 2020. It is because the IO warming dominates the atmospheric circulation anomalies over East Asia, including the meridional wind convergence (crucial for moisture convergence) and the enhanced westerly jets in the middle troposphere (essential for warm air advection and ascending motions) over the Meiyu-Baiu region. The situation in July, however, is quite different from that in June.

In July, the IO&ARCTIC experiment exhibits a meridional wind convergence due to anomalous southerlies and northerlies (Fig. 11c, d) and ascending motions associated with the warm advection associated with westerly anomalies over the Meiyu-Baiu region (Fig. 12d), which jointly results in enhanced rainfall over this region (Fig. 10f). Neither the IO nor the ARCTIC experiment is able to capture these atmospheric characteristics and precipitation anomaly patterns (Figs. 10g, h, 11c, d, 12e, f). In the IO experiment, from June into July, the anomalous WNPAC strengthens and extends northward and the anomalous Northeast Asian anticyclone moves eastward (Fig. 10c, g), which damages the PJ-like pattern in June. Accordingly, overwhelming southerlies (Fig. 11c) and descending motions (Fig. 12e) are found around the Meiyu-Baiu region in July.

By comparing the geopotential height responses in July between IO&ARCTIC and IO experiments (Fig. 10f, g), we can infer that the Arctic sea-ice loss is important to the dipole pattern in Northeast Asia in July. As expected, the ARCTIC experiment simulates a dipole pattern in Northeast Asia (Fig. 10h), which provides anomalous northerlies into the Meiyu-Baiu latitudes (Fig. 11c). The ARCTIC experiment also captures the positive westerly anomalies, leading

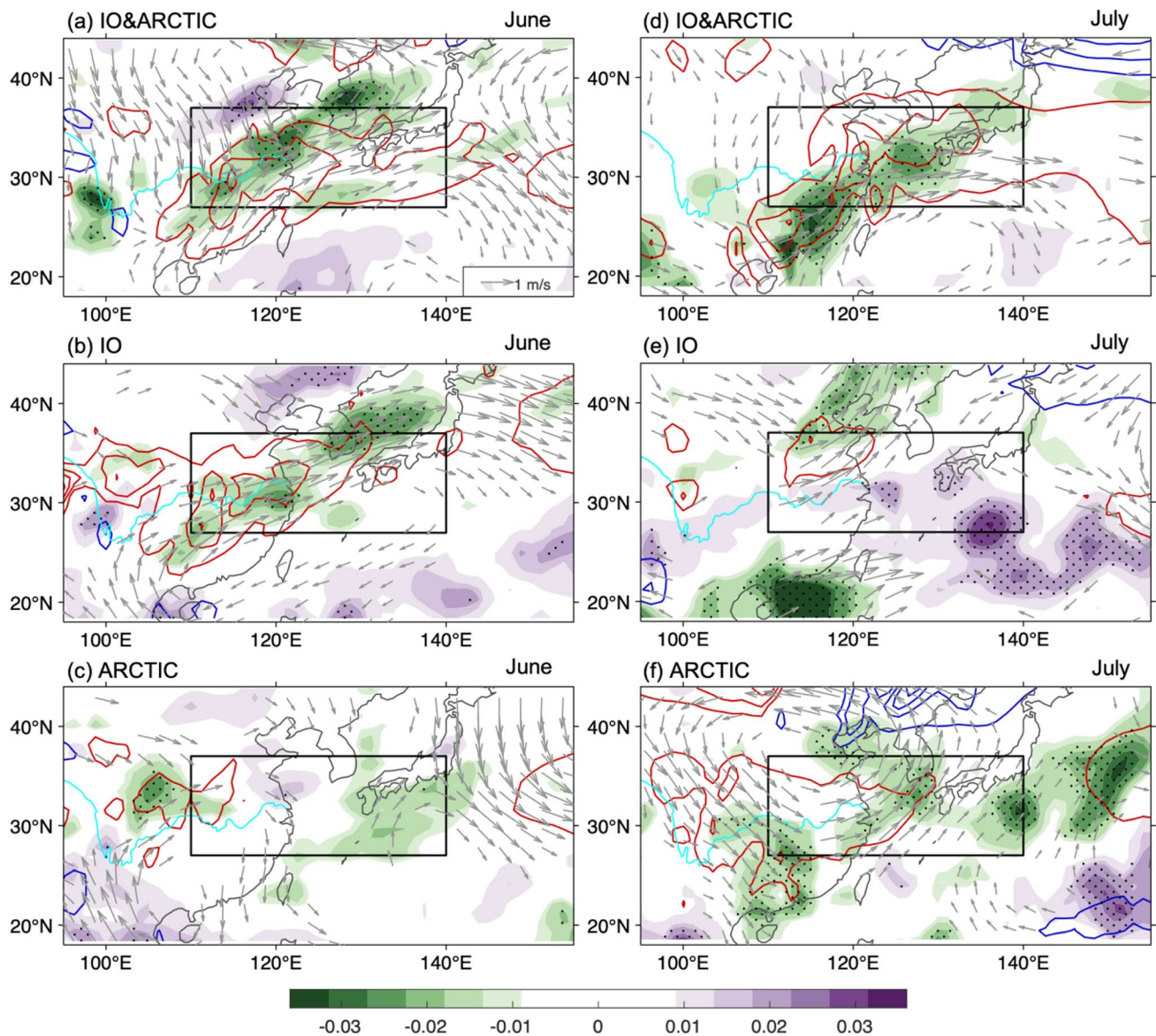


Fig. 12 Responses of 500 hPa vertical velocity (shading; Pa s^{-1}), horizontal winds (vectors; m s^{-1}), and zonal temperature advection (contours; interval = 10^{-5} K s^{-1} ; with red lines for warm advections and blue lines for cold advections, zero contour is omitted) in (left)

June and (right) July from (top) IO&ARCTIC, (middle) IO, and (bottom) ARCTIC experiments. The stippling indicates the significant vertical velocity anomaly. The black box highlights the Meiyu-Baiu region

to warm advection in the middle troposphere and ascending motions over the Meiyu-Baiu region (Fig. 12f). However, meridional wind convergence (Fig. 11d) and ascending motions (Fig. 12d, f) in the ARCTIC experiment are much weaker than that in the IO&ARCTIC experiment. The ascending response in the ARCTIC experiment spreads over a broader area compared with that in the IO&ARCTIC experiment (Fig. 12d, f). As a result, the precipitation response in the ARCTIC experiment not only increases in the Meiyu-Baiu region but also spreads over East China and the adjacent oceans (Fig. 10h). By comparing the geopotential height responses in July between IO&ARCTIC and

ARCTIC experiments (Fig. 10f, h), we find that the ARCTIC experiment fails to capture the anomalous WNPAC that can be generated by the IO warming (Fig. 10g). Without the anomalous WNPAC due to IO warming intensifying southerlies into the Meiyu-Baiu region, which interact with the Arctic-induced northerlies (Fig. 11c), the precipitation cannot be concentrated into a narrow belt from central-eastern China to Japan.

Thus, both IO warming and Arctic sea-ice loss are necessary for the heavy Meiyu-Baiu rainfall in July. As their effects are interdependent rather than additive, it is difficult to evaluate their relative importance. The Arctic sea-ice loss

and IO warming have never together reached such extreme states before 2020 (Fig. 2g, h), suggesting that the extremely heavy Meiyu-Baiu rainfall in 2020 might belong to an entirely new category in terms of causes. Both long-term trends and interannual variations contribute significantly to the 2020 extremes in IO warming and Arctic sea-ice loss (Fig. 2g, h). The interannual variations of IO SST and Arctic sea ice (red lines in Fig. 2g, h) are completely unrelated ($r=0.07$), suggesting a low probability of strong IO warming alongside severe Arctic sea-ice loss on the interannual timescale.

5 Conclusion and discussion

A record-breaking Meiyu-Baiu rainfall is observed in June–July 2020. The accumulated precipitation is particularly large in July, which is unexpected in the subseasonal to seasonal forecasting. This study investigates the cause of record-breaking Meiyu-Baiu rainfall in June and July of 2020 separately. We find that the excessive moisture convergence over the Meiyu-Baiu region in June and July 2020 was dynamically driven by meridional convergence of both northerly and southerly winds. The enhanced East Asian Westerly Jets results in anomalous warm advection in the mid-troposphere, which drives strong ascending motions. The meridional convergence and westerly anomalies are stronger in July, leading to heavier rainfall in July.

Modeling experiments suggest that IO warming generates an anomalous WNPAC and a negative PJ-like pattern in June, promoting meridional convergence and ascent over the Meiyu-Baiu region, which takes the primary responsibility for the enhanced rainfall in June. Meanwhile, the Arctic sea-ice loss favors a wave train pattern over the Eurasian high latitudes, including an anticyclone in Northeast Asia, but its impact on Meiyu-Baiu rainfall in June was minimal. In July, both IO warming and Arctic sea-ice loss are required to produce the meridional convergence, westerly anomalies, and enhanced precipitation over the Meiyu-Baiu region. Their effects are not linearly additive but interdependent. In the absence of Arctic sea-ice loss, the anomalous WNPAC induced by IO warming extends too far north, resulting in descending motions and reduced rainfall over the Meiyu-Baiu region. In the absence of IO warming, the meridional convergence, ascent, and enhanced rainfall caused by the Arctic sea-ice loss spread over East China and the surrounding seas instead of concentrating in the Meiyu-Baiu region.

Thus, the enhanced Meiyu-Baiu rainfall in June 2020 is mainly due to the strong IO warming, while the enhanced Meiyu-Baiu rainfall in July 2020 requires both the strong IO warming and the extreme Arctic sea-ice loss along the Siberian coast. Such a mechanism has not been documented

in historical heavy Meiyu-Baiu rainfalls, although many studies suggested impacts of sea-ice loss in the Norwegian and Barents Seas on East Asian precipitation (e.g., Wu et al. 2009, 2016; Shen et al. 2019; Zhang et al. 2021). Moreover, this mechanism of Arctic affecting East Asian precipitation is essentially different from the previous ones involving the North Atlantic Oscillation (e.g., Zhang et al. 2021) and Silk Road teleconnection (e.g., He et al. 2018).

Before 2020, pronounced IO warming is rarely observed alongside severe Arctic sea-ice loss due to their independent interannual variations. The long-term warming trend in the IO and the long-term decline trend in the Arctic sea ice contribute substantially to the extreme conditions in the IO and Arctic in the late spring and early summer of 2020. It partly explains why the extremely heavy Meiyu-Baiu rainfall in 2020 is so distinct. This study raises awareness about the influence of climate change on the midlatitude extreme events. As the long-term trends of IO warming and Arctic sea-ice loss continue, there is a growing possibility that we might experience severe Arctic sea-ice loss and extremely warm IO simultaneously, so their combined effect may become crucial in the future Meiyu-Baiu rainfall.

We realized that our simulations might not accurately reflect reality due to a considerable dampening effect from the use of fixed SST. The atmospheric response to the Arctic sea-ice loss might be underestimated due to an absence of air-sea interactions (Deser et al. 2015). Moreover, air-sea interactions in the North Pacific may prolong the atmospheric response (Guo et al. 2014). Nevertheless, this method has been widely used to examine atmospheric responses to tropical SST anomalies and Arctic sea-ice loss (e.g., Ding et al. 2014; Mori et al. 2014). Thus, our experiments are justified for providing qualitative information. Fully coupled model simulations are recommended in future studies.

Acknowledgements We appreciate the insightful suggestions from the two anonymous reviewers. This research was jointly supported by the National Natural Science Foundation of China (42105017) and China Postdoctoral Science Foundation (2020M681153, BX20200087). ZW acknowledges the support of National Natural Science Foundation of China grants (42030601, 41875087).

Open Access This article is licensed under a Creative Commons Attribution 4.0 International License, which permits use, sharing, adaptation, distribution and reproduction in any medium or format, as long as you give appropriate credit to the original author(s) and the source, provide a link to the Creative Commons licence, and indicate if changes were made. The images or other third party material in this article are included in the article's Creative Commons licence, unless indicated otherwise in a credit line to the material. If material is not included in the article's Creative Commons licence and your intended use is not permitted by statutory regulation or exceeds the permitted use, you will need to obtain permission directly from the copyright holder. To view a copy of this licence, visit <http://creativecommons.org/licenses/by/4.0/>.

References

- Ashok K, Behera SK, Rao SA, Weng H, Yamagata T (2007) El Niño Modoki and its possible teleconnection. *J Geophys Res* 112:C11007. <https://doi.org/10.1029/2006JC003798>
- Chen Y, Zhai P (2014) Precursor circulation features for persistent extreme precipitation in Central-Eastern China. *Weather Forecast* 29:226–240. <https://doi.org/10.1175/WAF-D-13-00065.1>
- Chen T, Zhang FH, Yu C, Ma J, Zhang XD, Shen XL, Zhang F, Luo Q (2020) Synoptic analysis of extreme Meiyu precipitation over Yangtze River Basin during June–July 2020. *Meteor Mon* 46:1415–1426 ((in chinese))
- Chen X, Dai A, Wen Z, Song Y (2021) Contributions of Arctic sea-ice loss and East Siberian atmospheric blocking to 2020 record-breaking Meiyu-Baiu rainfall. *Geophys Res Lett* 48:e2021GL092748. <https://doi.org/10.1029/2021GL092748>
- Chowdary JS, Xie SP, Luo J, Hafner J, Behera S, Masumoto Y, Yamagata T (2011) Predictability of Northwest Pacific climate during summer and the role of the tropical Indian Ocean. *Clim Dyn* 36:607–621. <https://doi.org/10.1007/s00382-009-0686-5>
- Ciavarella et al. (2020) Prolonged Siberian heat of 2020. <https://www.worldweatherattribution.org/wp-content/uploads/WWA-Prolonged-heat-Siberia-2020.pdf>
- Coumou D, Di Capua G, Vavrus S, Wang L, Wang S (2018) The influence of Arctic amplification on mid-latitude summer circulation. *Nat Commun* 9:2949. <https://doi.org/10.1038/s41467-018-05256-8>
- Dai A, Li H, Sun Y, Hong LC, Chou LC, Zhou T (2013) The relative roles of upper and lower tropospheric thermal contrasts and tropical influences in driving Asian summer monsoons. *J Geophys Res Atmos* 118:7024–7045
- Dai A, Luo D, Song M, Liu J (2019) Arctic amplification is caused by sea-ice loss under increasing CO₂. *Nat Commun* 10:121. <https://doi.org/10.1038/s41467-018-07954-9>
- Danabasoglu G, Lamarque JF, Bacmeister J et al (2020) The community earth system model Version 2 (CESM2). *J Adv Model Earth Syst* 12:e2019MS001916. <https://doi.org/10.1029/2019MS001916>
- Deser C, Tomas RA, Sun L (2015) The role of ocean–atmosphere coupling in the zonal-mean atmospheric response to Arctic sea ice loss. *J Clim* 28:2168–2186. <https://doi.org/10.1175/JCLI-D-14-00325.1>
- Ding Q, Wallace J, Battisti D et al (2014) Tropical forcing of the recent rapid Arctic warming in northeastern Canada and Greenland. *Nature* 509:209–212. <https://doi.org/10.1038/nature13260>
- Ding Y, Liang P, Liu Y, Zhang Y (2020) Multiscale variability of Meiyu and its prediction: a new review. *J Geophys Res: Atmos* 125:e2019JD031496. <https://doi.org/10.1029/2019JD031496>
- Ding Y, Liu Y, Hu Z (2021) The record-breaking Meiyu in 2020 and associated atmospheric circulation and tropical SST anomalies. *Adv Atmos Sci*. <https://doi.org/10.1007/s00376-021-0361-2>
- Fang C, Liu Y, CaiSong QH (2021) Why does extreme rainfall occur in central China during the summer of 2020 after a weak El Niño? *Adv Atmos Sci*. <https://doi.org/10.1007/s00376-021-1009-y>
- Guo D, Gao Y, Bethke I, Gong D, Johannessen OM, Wang H (2014) Mechanism on how the spring Arctic sea ice impacts the East Asian summer monsoon. *Theoret Appl Climatol* 115:107–119. <https://doi.org/10.1007/s00704-013-0872-6>
- Guo Y, Zhang R, Wen Z, Li J, Zhang C, Zhou Z (2021) Understanding the role of SST anomaly in extreme rainfall of 2020 Meiyu season from an interdecadal perspective. *Sci China Earth Sci*. <https://doi.org/10.1007/s11430-020-9762-0>
- He S, Gao Y, Furevik T, Wang H, Li F (2018) Teleconnection between sea ice in the Barents Sea in June and the Silk Road, Pacific–Japan and East Asian rainfall patterns in August. *Adv Atmos Sci* 35:52–64. <https://doi.org/10.1007/s00376-017-7029-y>
- Hersbach H, Bell B, Berrisford P et al (2020) The ERA5 global reanalysis. *Q J R Meteorol Soc* 146:1999–2049. <https://doi.org/10.1002/qj.3803>
- Huang R (1992) The East Asia/Pacific pattern teleconnection of summer circulation and climate anomaly in East Asia. *Acta Meteorol Sin* 6:25–37
- Huang R, Wu Y (1989) The influence of ENSO on the summer climate change in China and its mechanism. *Adv Atmos Sci* 6:21–32. <https://doi.org/10.1007/BF02656915>
- Kosaka Y, Xie SP, Nakamura H (2011) Dynamics of interannual variability in summer precipitation over East Asia. *J Clim* 24:5435–5453. <https://doi.org/10.1175/2011JCLI4099.1>
- Kucharski F, Biastoch A, Ashok K, Yuan D (2020) Indian Ocean Variability and Interactions. In: Mechoso C (eds) *Interacting Climates of Ocean basins: observations, mechanisms, predictability, and impacts* (pp 153–185). Cambridge University Press, Cambridge. <https://doi.org/10.1017/9781108610995.006>
- Li C, Lu R, Dunstone N, Scaife AA, Bett PE, Zheng F (2021) The seasonal prediction of the exceptional Yangtze River rainfall in Summer 2020. *Adv Atmos Sci* 38:2055–2066
- Liang P, Hu Z, Ding Y, Qian Q (2021) The extreme Mei-yu season in 2020: role of the Madden-Julian oscillation and the cooperative influence of the Pacific and Indian Oceans. *Adv Atmos Sci*. <https://doi.org/10.1007/s00376-021-1078-y>
- Liu B, Yan Y, Zhu C, Ma S, Li J (2020) Record-breaking Meiyu rainfall around the Yangtze River in 2020 regulated by the subseasonal phase transition of the North Atlantic Oscillation. *Geophys Res Lett* 47:e2020GL090342. <https://doi.org/10.1029/2020GL090342>
- Marathe S, Ashok K, Swapna P, Sabin TP (2015) Revisiting El Niño Modoki. *Clim Dyn* 45:3527–3545. <https://doi.org/10.1007/s00382-015-2555-8>
- Marathe S, Terray P, Karumuri A (2021) Tropical Indian Ocean and ENSO relationships in a changed climate. *Clim Dyn* 56:3255–3276. <https://doi.org/10.1007/s00382-021-05641-y>
- Mori M, Watanabe M, Shiogama H, Inoue J, Kimoto M (2014) Robust Arctic sea-ice influence on the frequent Eurasian cold winters in past decades. *Nat Geosci* 7:869–873. <https://doi.org/10.1038/ngeo2277>
- NASA (2020) IMERG measures flooding rainfall from "Plum Rains" in Japan. <https://gpm.nasa.gov/applications/weather/imerg-measures-flooding-rainfall-plum-rains-japan>
- Ninomiya K, Akiyama T (1992) Multi-scale Features of Baiu, the summer monsoon over Japan and the East Asia. *J Meteorol Soc Jpn Ser II* 70:467–495. https://doi.org/10.2151/jmsj1965.70.1B_467
- Nitta T (1987) Convective activities in the tropical western Pacific and their impact on the Northern Hemisphere summer circulation. *J Meteorol Soc Jpn* 65:373–390. https://doi.org/10.2151/jmsj1965.65.3_373
- NSIDC (2020a) Laptev Sea lapping up the heat in June. <https://nsidc.org/arcticseai cenews/2020a/07/laptev-sea-lapping-up-the-heat-in-june/>
- NSIDC (2020b) Siberian downward slide. <http://nsidc.org/arcticseai cenews/2020b/07/siberian-downward-slide/>
- Okada Y, Yamazaki K (2012) Climatological evolution of the Okinawa baiu and differences in large-scale features during May and June. *J Clim* 25(18):6287–6303
- Overland JE, Wang M (2020) The 2020 Siberian heat wave. *Int J Climatol* 41:E2341–E2346. <https://doi.org/10.1002/joc.6850>
- Pan X, Li T, Sun Y, Zhu Z (2021) Cause of extreme heavy and persistent rainfall over Yangtze River in summer 2020. *Adv Atmos Sci*. <https://doi.org/10.1007/s00376-021-0433-3>
- Qiao S, Chen D, Wang B, Cheung HN, Liu F, Cheng J, Tang S, Zhang Z, Feng G, Dong W (2021) The longest 2020 Meiyu season over the past 60 years: subseasonal perspective and its predictions.

- Geophys Res Lett 48:e2021GL093596. <https://doi.org/10.1029/2021GL093596>
- Ratna SB, Cherchi A, Osborn TJ, Joshi M, Uppara U (2021) The extreme positive Indian Ocean dipole of 2019 and associated indian summer monsoon rainfall response. *Geophys Res Lett* 48:e2020GL091497
- Saji NH (2018) The Indian Ocean dipole. *Oxford research encyclopedia. Clim Sci* 35:25. <https://doi.org/10.1093/acrefore/9780190228620.013.619>
- Saji NH, Xie SP, Yamagata T (2006) Tropical Indian Ocean variability in the IPCC twentieth-century climate simulations. *J Clim* 19(17):4397–4417
- Saji N, Goswami B, Vinayachandran P et al (1999) A dipole mode in the tropical Indian Ocean. *Nature* 401:360–363. <https://doi.org/10.1038/43854>
- Sampe T, Xie SP (2010) Large-scale dynamics of the meiyu-baiu rainband: environmental forcing by the westerly jet. *J Clim* 23:113–134. <https://doi.org/10.1175/2009JCLI3128.1>
- Seager R, Henderson N (2013) Diagnostic computation of moisture budgets in the ERA-Interim reanalysis with reference to analysis of CMIP-archived atmospheric model data. *J Clim* 26:7876–7901. <https://doi.org/10.1175/JCLI-D-13-00018.1>
- Shen H, He S, Wang H (2019) Effect of summer Arctic sea ice on the reverse August precipitation anomaly in eastern China between 1998 and 2016. *J Clim* 32:3389–3407. <https://doi.org/10.1175/JCLI-D-17-0615.1>
- Steffing J, Semmler T, Zampieri L, Jung T (2021) Response of Northern Hemisphere weather and climate to Arctic Sea Ice decline: resolution Independence in polar amplification model intercomparison project (PAMIP) simulations. *J Clim* 34:8445–8457. <https://doi.org/10.1175/JCLI-D-19-1005.1>
- Takaya Y, Ishikawa I, Kobayashi C, Endo H, Ose T (2020) Enhanced Meiyu-Baiu rainfall in early summer 2020: Aftermath of the 2019 super IOD event. *Geophys Res Lett* 47:90671. <https://doi.org/10.1029/2020GL090671>
- Tanaka M (1997) Interannual and interdecadal variations of the western North Pacific monsoon and Baiu rainfall and their relationship to the ENSO cycles. *J Meteorol Soc Jpn Ser II* 75:1109–1123. https://doi.org/10.2151/jmsj1965.75.6_1109
- Tang Q, Zhang X, Francis JA (2014) Extreme summer weather in northern mid-latitudes linked to a vanishing cryosphere. *Nat Clim Change* 4:45–50. <https://doi.org/10.1038/nclimate2065>
- Tang S, Luo J, He J, Wu J, Zhou Y, Ying W (2021) Toward understanding the extreme floods over Yangtze River Valley in June–July 2020: role of tropical Oceans. *Adv Atmos Sci*. <https://doi.org/10.1007/s00376-021-1036-8>
- Tao S, Chen L (1987) A review of recent research on the East Asia summer monsoon over China in Monsoon meteorology. Oxford university Press, Oxford, pp 50–92
- Ueda H, Yokoi M, Kuramochi M (2021) Enhanced subtropical anticyclone over the Indo-Pacific Ocean associated with stagnation of the Meiyu-Baiu rainband during summer, 2020. *SOLA*. <https://doi.org/10.2151/sola.17B-002>
- Wang L, Sun X, Yang X, Tao L, Zhang Z (2021) Contribution of water vapor to the record-breaking extreme Meiyu rainfall along the Yangtze River Valley in 2020. *J Meteorol Res* 35:557–570. <https://doi.org/10.1007/s13351-021-1030-1>
- Wu B, Zhang R, Wang B, D'Arrigo R (2009) On the association between spring Arctic sea ice concentration and Chinese summer rainfall. *Geophys Res Lett* 36:L09501. <https://doi.org/10.1029/2009GL037299>
- Wu Z, Li X, Li Y, Li Y (2016) Potential influence of Arctic sea ice to the interannual variations of East Asian spring precipitation. *J Clim* 29:2797–2813. <https://doi.org/10.1175/JCLI-D-15-0128.1>
- Xie SP, Hu K, Hafner J, Tokinaga H, Du Y, Huang G, Sampe T (2009) Indian Ocean capacitor effect on Indo-Western pacific climate during the summer following El Nino. *J Clim* 22:730–747. <https://doi.org/10.1175/2008JCLI2544.1>
- Yang J, Liu Q, Xie SP, Liu Z, Wu L (2007) Impact of the Indian Ocean SST basin mode on the Asian summer monsoon. *Geophys Res Lett* 34:L02708. <https://doi.org/10.1029/2006GL028571>
- Zhang P, Wu Z, Jin R (2021) How can the winter North Atlantic Oscillation influence the early summer precipitation in Northeast Asia: effect of the Arctic sea ice. *Clim Dyn* 56:1989–2005. <https://doi.org/10.1007/s00382-020-05570-2>
- Zheng JY, Wang CZ (2021) Influences of three oceans on record-breaking rainfall over the Yangtze River Valley in June 2020. *Sci China Earth Sci*. <https://doi.org/10.1007/s11430-020-9758-9>
- Zhou Z, Xie S, Zhang R (2021) Historic Yangtze flooding of 2020 tied to extreme Indian Ocean conditions. *Proc Georgian Natl Acad Sci* 118:e2022255118. <https://doi.org/10.1073/pnas.2022255118>

Publisher's Note Springer Nature remains neutral with regard to jurisdictional claims in published maps and institutional affiliations.